Eur. Phys. J. C 44, 277–286 (2005)
Digital Object Identifier (DOI) 10.1140/epjc/s2005-02361-3

THE EUROPEAN PHYSICAL JOURNAL C

Study of a neutrino mass texture generated in supergravity with bilinear R-parity violation

M.A. Díaz[1,a], C. Mora[1], A.R. Zerwekh[2,3]

[1] Departamento de Física, Universidad Católica de Chile, Avenida Vicuña Mackenna 4860, Santiago, Chile
[2] Departamento de Física, Universidad Técnica Federico Santa María, Casilla 110-V, Valparaiso, Chile
[3] Instituto de Física, Universidad Austral de Valdivia, Casilla 567, Valdivia, Chile

Received: 29 October 2004 / Revised version: 8 July 2005 /
Published online: 13 September 2005 –

Abstract. We study a particular texture of the neutrino mass matrix generated in supergravity with non-universal bilinear R-parity violation parameters. The relatively high value of $\tan\beta$ makes the one-loop contribution to the neutrino mass matrix as important as the tree-level one. The atmospheric angle is nearly maximal, and its deviation from maximal mixing is related to the small size of the ratio between the solar and atmospheric mass scales. There is also a common origin for the small values of the solar and reactor angles, but the latter is much smaller due the large mass ratio between the heaviest two neutrinos. There is a high dependence of the neutrino mass differences on the scalar mass m_0 and the gaugino mass $M_{1/2}$, but a smaller dependence of the mixing angles on the same Sugra parameters. Measurements of branching ratios for the neutralino decays can give important information on the parameters of the model. There are good prospects at a future linear collider for these measurements, but a more detailed analysis is necessary for the LHC.

1 Introduction

With a number of experimental results in atmospheric, solar, reactor, and accelerator neutrino physics, it has been established that neutrinos have mass and oscillate [1]. This is a very important result in itself but, in addition, it is the first direct experimental indication that the standard model (SM) needs to be modified [2].

In the SM, neutrinos are massless. One popular mechanism for the generation of neutrino masses is the see-saw mechanism, where a right-handed neutrino field with a very large mass is added to the SM [3]. The resulting neutrino mass is inversely proportional to this large mass. Another interesting and predictive mechanism is the radiative generation of neutrino masses and mixing in a supersymmetric model [4] that violates lepton number and R-parity [5] with bilinear terms in the superpotential. Phenomenological consequences of R-parity-violating supersymmetry are very distinct from R-parity-conserving models [6].

Bilinear R-parity breaking is an interesting mechanism for the generation of neutrino masses and mixing angles due to its simplicity and predictability [7,8]. It is a simple extension of the minimal supersymmetric standard model (MSSM) which includes no new fields and no new interactions. It differs from the MSSM in a handful of bilinear terms that violate lepton number and R-parity, which cannot be eliminated with field redefinitions [9]. Neutrino masses and mixing angles are calculable and agree with experimental measurements [10,11]. Motivations for bilinear R-parity violation (BRpV) are, for example, models with spontaneously broken R-parity [12], and a model with an anomalous horizontal $U(1)$ symmetry [13], where BRpV appears without trilinear R-parity violation.

Results from SuperKamiokande [1] on atmospheric neutrinos gave strong evidence of the ν_μ–ν_τ oscillation of atmospheric neutrinos with maximal or nearly maximal mixing, and gave strong evidence against the small-mixing-angle solution of the solar neutrino problem. Results from the Sudbury Neutrino Observatory (SNO) and the KamLAND experiment have confirmed the large-mixing-angle solution of the solar neutrino problem, showing that more than half of the electron neutrinos produced at the sun oscillate into other flavors before reaching the Earth [1]. Results from the Wilkinson microwave anisotropy probe (WMAP) show temperature differences within the microwave background radiation, which combined with results from large scale structure give a bound on the sum of the neutrino masses [14]. Finally, evidence for neutrinoless double-beta decay, if confirmed, would show the Majorana nature of neutrinos and the non-conservation of lepton numbers [15].

There are several analysis of these experimental results [16]. The 3σ allowed regions for the neutrino parameters in [17] are

$$1.4 \times 10^{-3} < \Delta m^2_{32} < 3.3 \times 10^{-3}\,\mathrm{eV}^2$$

[a] e-mail: mad@susy.fis.puc.cl

$$\begin{aligned} 7.2\times10^{-5} < \ \Delta m^2_{21} \ &< 9.1\times10^{-5}\,\mathrm{eV}^2 \\ 0.52 < \tan^2\theta_{23} &< 2.1 \\ 0.30 < \tan^2\theta_{12} &< 0.61 \\ \tan^2\theta_{13} &< 0.049 \end{aligned} \tag{1}$$

which we show for reference.

In this article, we reanalyze the possibility of having BRpV in a supergravity scenario, in which the scalar masses and the gaugino masses are universal at the grand unified theory GUT scale. The electroweak symmetry is broken radiatively but, contrary to the MSSM, sneutrinos acquire vacuum expectation values as well as the Higgs bosons. We give up the possibility that the ϵ_i and B_i parameters (one for each lepton analogously to the μ and B terms in the MSSM respectively) are universal at the GUT scale, because otherwise there is no good solution for neutrino physics that is compatible with experiments.

We found solutions that have not been discussed previously in the literature. These solutions are characterized by a large value of $\tan\beta$ and, therefore, the importance of one-loop contributions to the neutrino mass matrix is enhanced.

2 Neutrino mass at tree level

The superpotential of our BRpV model differs from the MSSM by three terms which violate R-parity and lepton number,

$$W = W_{MSSM} + \epsilon_i \hat{L}_i \hat{H}_u \tag{2}$$

where the ϵ_i have units of mass. We complement these with related terms in the soft Lagrangian,

$$\mathcal{L} = \mathcal{L}_{MSSM} + B_i \epsilon_i \widetilde{L}_i H_u \tag{3}$$

where the B_i also have units of mass. The presence of these terms induce vacuum expectation values v_i for the sneutrinos, which are calculated by minimizing the scalar potential.

At the tree level, neutrino masses are generated via a low-energy see-saw-type mechanism. Neutrinos mix with neutralinos, and the MSSM neutralino mass matrix is expanded to a 7×7 mass matrix for the neutral fermions

$$\mathbf{M}_N = \begin{bmatrix} \mathcal{M}_{\chi^0} & m^T \\ m & 0 \end{bmatrix} . \tag{4}$$

Here, $\mathcal{M}_{\chi^0}$ is the usual 4×4 neutralino mass matrix, and m is

$$m = \begin{bmatrix} -\frac{1}{2}g'v_1 & \frac{1}{2}gv_1 & 0 & \epsilon_1 \\ -\frac{1}{2}g'v_2 & \frac{1}{2}gv_2 & 0 & \epsilon_2 \\ -\frac{1}{2}g'v_3 & \frac{1}{2}gv_3 & 0 & \epsilon_3 \end{bmatrix} \tag{5}$$

which mixes the neutrinos with the neutralinos. The matrix $\mathbf{M}_N$ can be diagonalized by blocks, and the effective 3×3 neutrino mass matrix turns out to be equal to

$$\mathbf{M}_\nu^{(0)} = -\, m\cdot\mathcal{M}_{\chi^0}^{-1}\cdot m^T$$

$$= \frac{M_1 g^2 + M_2 g'^2}{4\,det(\mathcal{M}_{\chi^0})} \begin{bmatrix} \Lambda_1^2 & \Lambda_1\Lambda_2 & \Lambda_1\Lambda_3 \\ \Lambda_1\Lambda_2 & \Lambda_2^2 & \Lambda_2\Lambda_3 \\ \Lambda_1\Lambda_3 & \Lambda_2\Lambda_3 & \Lambda_3^2 \end{bmatrix} \tag{6}$$

where we have defined the parameters $\Lambda_i = \mu v_i + \epsilon_i v_d$, which are proportional to the sneutrino vacuum expectation values in the basis where the ϵ terms are removed from the superpotential.

This mass matrix can be diagonalized with the following two rotations.

$$V_\nu^{(0)} = \begin{pmatrix} 1 & 0 & 0 \\ 0 & \cos\theta_{23}^{(0)} & -\sin\theta_{23}^{(0)} \\ 0 & \sin\theta_{23}^{(0)} & \cos\theta_{23}^{(0)} \end{pmatrix} \times \begin{pmatrix} \cos\theta_{13}^{(0)} & 0 & -\sin\theta_{13}^{(0)} \\ 0 & 1 & 0 \\ \sin\theta_{13}^{(0)} & 0 & \cos\theta_{13}^{(0)} \end{pmatrix} , \tag{7}$$

where the reactor mixing angle in terms of the *alignment vector* $\boldsymbol{\Lambda}$ is

$$\tan\theta_{13}^{(0)} = -\frac{\Lambda_1}{(\Lambda_2^2+\Lambda_3^2)^{\frac{1}{2}}} , \tag{8}$$

and the atmospheric angle is

$$\tan\theta_{23}^{(0)} = \frac{\Lambda_2}{\Lambda_3} . \tag{9}$$

As we will see later, despite the fact that the tree-level contribution to the heavy neutrino mass dominates over all loops, there are other contributions to the neutrino mass matrix that cannot be neglected. For this reason, the above tree-level formulas will not be enough to explain the results.

3 Supergravity and BRpV

In Sugra–BRpV the independent parameters are

$$m_0\,, M_{1/2}\,, A_0\,, \tan\beta\,, \mathrm{sign}(\mu)\,, \epsilon_i\,, \Lambda_i\,, \tag{10}$$

where m_0 is the universal scalar mass, $M_{1/2}$ is the universal gaugino mass, and A_0 is the universal trilinear coupling, valid at the GUT scale. In addition, $\tan\beta$ is the ratio between the Higgs vacuum expectation values, and $\mathrm{sign}(\mu)$ is the sign of the Higgsino mass parameter, both valid at the EWSB scale. Finally, ϵ_i are the supersymmetric BRpV parameters in the superpotential, and Λ_i the parameters depending on the sneutrino vacuum expectation values.

As we mentioned in the Introduction, the scenario with universal ϵ_i and B_i terms at the GUT scale is excluded by neutrino experiments; thus, we relax it. In this way, we use ϵ_i and B_i at the weak scale as free parameters. The minimization conditions for the scalar potential are

$$\begin{aligned} 0 &= \left(m_{H_d}^2+\mu^2\right)v_d + v_d D - \mu\left(B_0 v_u + \boldsymbol{v}\cdot\boldsymbol{\epsilon}\right) , \\ 0 &= -B_0\mu v_d + \left(m_{H_u}^2+\mu^2\right)v_u - v_u D + \boldsymbol{v}\cdot\boldsymbol{B}_\epsilon + v_u\boldsymbol{\epsilon}^{\,2} , \\ 0 &= v_i D + \epsilon_i\left(-\mu v_d + v_u B_i + \boldsymbol{v}\cdot\boldsymbol{\epsilon}\right) + v_i M_{Li}^2 , \end{aligned} \tag{11}$$

where $D = \frac{1}{8}(g^2+g'^2)(v_d^2 - v_u^2 + \boldsymbol{v}^{\,2})$, $(\boldsymbol{v})_i = v_i$, $(\boldsymbol{\epsilon})_i = \epsilon_i$, and $(\boldsymbol{B}_\epsilon)_i = B_i\epsilon_i$. From these equations we calculate the sneutrino vacuum expectation values as a function of the soft and supersymmetric (SUSY) terms.

We use the code SUSPECT [18] to run the two loops RGE from the unification scale down to the weak scale. The electroweak symmetry breaking is analogous to the MSSM, with the difference that there are three extra vacuum expectation values (VEV) corresponding to the sneutrino VEVs v_i. These VEVs are small and constitute a small perturbation to the MSSM EWSB.

Despite the fact that sneutrino VEVs are dependent quantities, since they are calculated from the minimization of the scalar potential, we remove from the group of independent parameters the B_is in favor of $\Lambda_i = \mu v_i + \epsilon_i v_d$, as indicated in (10), because they are more useful in describing the neutrino physics. As in the MSSM, the input parameters B_0 and $|\mu|$ are eliminated in favor of $\tan\beta$ and m_z. In a similar fashion, in BRpV the input parameters B_i are eliminated in favor of v_i (or more precisely, in favor of Λ_i), explaining our choice of free parameters in (10).

Our analysis will be centered around the SPS1 scenario in Sugra from the Snowmass 2001 benchmark scenarios [19], which is defined by

$$\begin{aligned} &m_0 = 100\,\mathrm{GeV}\,, \quad M_{1/2} = 250\,\mathrm{GeV}\,, \\ &A_0 = -100\,\mathrm{GeV}\,, \quad \tan\beta = 10\,, \quad \mu > 0\,. \end{aligned} \tag{12}$$

This scenario is typical of Sugra, with a neutralino lightest supersymmetric particle (LSP) with a mass of $m_{\chi_1^0} = 99\,\mathrm{GeV}$, and a light neutral Higgs boson with a mass just above the experimental limit $m_h = 114\,\mathrm{GeV}$.

In this context we find several solutions for neutrino physics which satisfy the experimental constraints on the atmospheric and solar mass squared differences, the three mixing angles, and the mass parameter associated with neutrinoless double-beta decay [20]. For illustrative purposes we single out the following

$$\begin{aligned} &\epsilon_1 = -0.0004\,, \quad \epsilon_2 = 0.052\,, \quad \epsilon_3 = 0.051\,, \\ &\Lambda_1 = 0.022\,, \quad \Lambda_2 = 0.0003\,, \quad \Lambda_3 = 0.039\,. \end{aligned} \tag{13}$$

This solution is characterized by

$$\begin{aligned} &\Delta m^2_{32} = 2.7\times10^{-3}\,\mathrm{eV}^2\,, \quad \Delta m^2_{21} = 8.1\times10^{-5}\,\mathrm{eV}^2\,, \\ &m_{ee} = 0.0036\,\mathrm{eV}\,, \quad \tan^2\theta_{23} = 0.72\,, \\ &\tan^2\theta_{12} = 0.54\,, \quad \tan^2\theta_{13} = 0.0058\,, \end{aligned} \tag{14}$$

which are well inside the experimentally allowed window in (1). We note that the random solution in (13) is compatible with $\epsilon_1 = \Lambda_2 = 0$, that is, the neutrino parameters in (14) are hardly changed with this replacement.

As seen in the following chapters the model is highly constrained, but as a consequence it is also highly predictive. If parameters are varied randomly within $|\epsilon_i|^2, |\Lambda_i| < 1\,\mathrm{GeV}^2$, good solutions are found every 10^3–10^4 points. Nevertheless, this should not be interpreted as a sign of fine-tuning, because the real cause is the high precision of the experimental results in neutrino observations. In this sense, the constraints on the sneutrino VEVs imposed by neutrino experiments can be considered as analogous to the constraints on the Higgs VEVs imposed by gauge-boson mass measurements.

4 Texture of the neutrino mass matrix

Among the solutions to neutrino physics that we have found in our model, there are a few textures [22] for the effective neutrino mass matrix. Our study case in (13) belongs to the most frequent one, which is

$$\mathbf{M}_\nu^{eff} = m \begin{bmatrix} \lambda & 0 & \lambda \\ 0 & a & a \\ \lambda & a & 1 \end{bmatrix} \tag{15}$$

with $a \sim 0.5$–0.8, $\lambda \sim 0.1$–0.3, and $m \sim 0.02$–$0.04\,\mathrm{eV}$. To understand how this texture works we expand the neutrino masses and mixing angles in powers of λ. Keeping terms up to first order, the three neutrino masses are

$$\begin{aligned} m_{\nu_1} &= \lambda m + \mathcal{O}(\lambda^2) \\ m_{\nu_2} &= \tfrac{1}{2} m(1 + a - \sqrt{5a^2 - 2a + 1}) + \mathcal{O}(\lambda^2) \\ m_{\nu_3} &= \tfrac{1}{2} m(1 + a + \sqrt{5a^2 - 2a + 1}) + \mathcal{O}(\lambda^2) \end{aligned} \tag{16}$$

and the rotation matrix that diagonalizes the neutrino mass matrix, denoted by U_{PMNS}, is

$$U_{\mathrm{PMNS}} = \begin{bmatrix} 1 & \lambda s_\theta m/m_{\nu_2} & \lambda c_\theta m/m_{\nu_3} \\ \lambda/(1-a) & c_\theta & -s_\theta \\ -\lambda/(1-a) & s_\theta & c_\theta \end{bmatrix} + \mathcal{O}(\lambda^2) \tag{17}$$

with

$$\tan 2\theta = \frac{-2a}{1-a}\,. \tag{18}$$

In the same approximation, the atmospheric, solar, and reactor angles are given by

$$\begin{aligned} \tan 2\theta_{23} &= 2a/(1-a) + \mathcal{O}(\lambda^2) \\ \tan\theta_{12} &= \lambda s_\theta m/m_{\nu_2} + \mathcal{O}(\lambda^2) \\ \sin\theta_{13} &= \lambda c_\theta m/m_{\nu_3} + \mathcal{O}(\lambda^2) \end{aligned} \tag{19}$$

while the atmospheric and solar mass differences are

$$\begin{aligned} \Delta m^2_{32} &= m^2(1+a)\sqrt{5a^2 - 2a + 1} + \mathcal{O}(\lambda^2)\,, \\ \Delta m^2_{21} &= \tfrac{1}{2} m^2 \left[1 + 3a^2 - (1+a)\sqrt{5a^2 - 2a + 1}\right] \\ &\quad + \mathcal{O}(\lambda^2)\,. \end{aligned} \tag{20}$$

As an example, consider $a = 1/2$ and $m = 0.04\,\mathrm{eV}$. We find $\Delta m^2_{32} = 3\sqrt{5}m^2/4 \approx 2.7\times10^{-3}\,\mathrm{eV}^2$, and $\Delta m^2_{21} = (7 - 3\sqrt{5})m^2/8 \approx 5.8\times10^{-5}\,\mathrm{eV}^2$, both in agreement with experiments. The third parameter, which in this approximation does not depend on the small parameter λ, is the atmospheric angle, obtaining $\tan^2\theta_{23} \approx 0.4$ from (18). This

value is at the lower end of the allowed region, nevertheless, taking $a = 0.6$ we obtain $\tan^2\theta_{23} \approx 0.5$, which is in better agreement with experiments.

The fact that a is smaller than unity implies that the atmospheric mixing is not maximal. In the limit $a \to 1$, the atmospheric mixing approaches maximality, but the atmospheric mass $\Delta m^2_{atm} \to 4m^2$ which is too large if $m = 0.04\,\mathrm{eV}$, and the solar mass $\Delta m^2_{sol} \to 0$, which is too small. Decreasing $\tan^2\theta_{atm}$ by decreasing a will decrease the atmospheric mass scale and increase the solar one, both towards acceptable values. Therefore, the value of a relates these three neutrino parameters, such that the non-maximal value for the atmospheric angle is connected to the smallness of the ratio between the solar mass scale and the atmospheric scale.

The previous considerations are modified by the non-zero value of λ. In the approximation to which we are working, the solar and reactor angles are proportional to the parameter λ, thus they are small quantities themselves. Nevertheless, the presence of m_{ν_2} in the denominator of $\tan\theta_{12}$, as opposed to m_{ν_3} in the denominator of $\tan\theta_{13}$, makes the reactor angle much smaller than the solar angle. In the case $a = 1/2$ and $\lambda = 0.2$ we find for the solar angle $\tan^2\theta_{12} = 0.3$, which is in the lower part of the allowed region and compatible with experiments. For the reactor angle we find $\tan^2\theta_{13} = 0.017$ which is well below the experimental upper bound. We stress that we use the complete numerical calculation in the rest of the article, rather than these approximated formulas.

5 One-loop contributions

All particles in the MSSM contribute to the renormalization of the neutralino/neutrino mass matrix. One of the most important contributions comes from the bottom–sbottom loops. In the gauge eigenstate basis this contribution is [21],

$$\Delta\Pi_{ij} = -\frac{N_c m_b}{16\pi^2} 2 s_{\tilde{b}} c_{\tilde{b}} h_b^2 \Delta B_0^{\tilde{b}_1\tilde{b}_2} \times \left[\frac{\epsilon_i\epsilon_j}{\mu^2} - \frac{a_3}{\mu}(\epsilon_i\Lambda_j + \epsilon_j\Lambda_i) + \left(a_3^2 + \frac{a_L a_R}{h_b^2}\right)\Lambda_i\Lambda_j\right] \tag{21}$$

where we have defined

$$a_R = \frac{g}{\sqrt{2}}\left(\frac{1}{3}t_W a_1 - a_2\right), \qquad a_L = \frac{g}{\sqrt{2}}\,\frac{2}{3}t_W a_1\,, \tag{22}$$

$$\begin{aligned} a_1 &= \frac{g' M_2 \mu}{2\Delta_0}\,, \qquad a_2 = -\frac{g M_1 \mu}{2\Delta_0}\,, \\ a_3 &= \frac{v_u}{4\Delta_0}(g^2 M_1 + g'^2 M_2)\,. \end{aligned} \tag{23}$$

The main contributions to (21) can be understood as coming from the graph

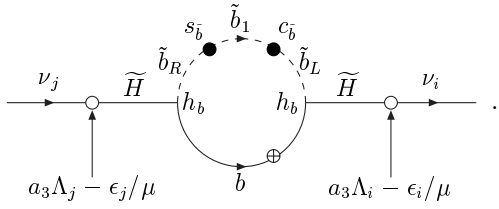

Here, neutrinos (in the gauge eigenstate basis) mix with Higgsinos, which in turn interact with the pair bottom–sbottom with a strength proportional to the corresponding Yukawa coupling. Full circles indicate the projection of the sbottom mass eigenstate into right and left sbottom, which contribute with a $\sin\theta_{\tilde{b}}$ and $\cos\theta_{\tilde{b}}$ respectively. Open circles indicate the projection of the neutrino field onto the Higgsino, proportional to the small parameter $a_3\Lambda_i - \epsilon_i/\mu$. The quark propagator contributes with a factor m_b, and summing over color gives the factor N_c. Finally, we have in (21)

$$\Delta B_0^{\tilde{b}_1\tilde{b}_2} \equiv B_0\left(0, m^2_{\tilde{b}_1}, m_b^2\right) - B_0\left(0, m^2_{\tilde{b}_2}, m_b^2\right). \tag{24}$$

The one-loop corrected neutrino mass matrix, in the first approximation, has the general form

$$\Delta\Pi_{ij} = A\Lambda_i\Lambda_j + B(\epsilon_i\Lambda_j + \epsilon_j\Lambda_i) + C\epsilon_i\epsilon_j \tag{25}$$

since all loop contributions can be expanded in this way. The terms of higher order in Λ and ϵ have been neglected.

Considering the solutions to neutrino physics whose effective neutrino mass matrix has a texture of the form in (15), and including contributions from all one-loop graphs, we extract the numerical value of the above parameters and find $A \approx 7\,\mathrm{eV/GeV^4}$, $B \approx -0.5\,\mathrm{eV/GeV^3}$, and $C \approx 9\,\mathrm{eV/GeV^2}$.

Of the three parameters only A gets a contribution at tree level, and we estimate

$$A^{(0)} = \frac{g^2 M_1 + g'^2 M_2}{4\Delta_0} \approx 7.6\,\mathrm{eV/GeV^4}\,. \tag{26}$$

Clearly, the tree-level contribution to A dominates over all one-loop graphs. This is not true for B and C because these two parameters are entirely generated at one loop.

The contribution to A, B, and C from the bottom–sbottom loops can be read from (21). In the squark sector we have $m_{\tilde{b}_1} = 492$, $m_{\tilde{b}_2} = 538\,\mathrm{GeV}$, and $\sin 2\theta_{\tilde{b}} = 0.88$, which implies

$$C^{(1)}_{\tilde{b}} = -\frac{N_c m_b}{8\pi^2\mu^2} s_{\tilde{b}} c_{\tilde{b}} h_b^2 \Delta B_0^{\tilde{b}_1\tilde{b}_2} \approx 9.8\,\mathrm{eV/GeV^2}\,. \tag{27}$$

This result is very close to the actual numerical value, and underlines the fact that the bottom–sbottom loops are very important in this particular scenario.

Considering that the value for B, in the supergravity model with which we are working, is much smaller than A and C, we might in first approximation neglect it in (25). In this case, for the neutrino solution in (13) we obtain the following approximated neutrino mass matrix,

$$\mathbf{M}_\nu^{eff} = \begin{bmatrix} A\Lambda_1^2 & 0 & A\Lambda_1\Lambda_3 \\ 0 & C\epsilon_2^2 & C\epsilon_2\epsilon_3 \\ A\Lambda_1\Lambda_3 & C\epsilon_2\epsilon_3 & A\Lambda_3^2 + C\epsilon_3^2 \end{bmatrix}. \tag{28}$$

This form is precisely the texture observed in (15) obtained from the numerical results. Therefore, the zero in the neutrino mass matrix is there because $\Lambda_2, \epsilon_1 \approx 0$ and because

B is very small compared with A and C. The three matrix elements of order λ in (15) are explained by the fact that Λ_1 has a numerical value smaller than the other three relevant parameters, as can be seen from (13). Finally, the parameter a in (15) is smaller than unity because $A\Lambda_3^2$ and $C\epsilon_3^2$ are comparable and of the same sign, and because $\epsilon_2 \approx \epsilon_3$.

6 Numerical results

In this section we study numerical results on the neutrino mass matrix, neutrino mass differences and mixing angles. We center our studies in the supergravity benchmark given in (12), although we also explore the behavior of the neutrino parameters in the $m_0 - M_{1/2}$ plane. We look for solutions to neutrino physics with different values of the BRpV parameters ϵ_i and Λ_i, but concentrate our attention in the particular solution given in (13).

First, we consider the supergravity benchmark in (12) and randomly vary the BRpV parameters ϵ_i and Λ_i. We look for solutions satisfying experimental restrictions on neutrino parameters according to the 3σ intervals in (1), and also according to a relaxation of those cuts given by:

$$\begin{aligned} 1.2 \times 10^{-3} < \ & \Delta m^2_{32} \ < 4.8 \times 10^{-3}\,\mathrm{eV}^2 \\ 0.43 < \ & \tan^2\theta_{23} < 2.3 \\ 5.1 \times 10^{-5} < \ & \Delta m^2_{21} \ < 19 \times 10^{-5}\,\mathrm{eV}^2 \end{aligned} \tag{29}$$

motivated by previous allowed regions and shown to compare the effect of the improved analysis of the experimental data.

Solutions satisfying the relaxed cuts given in (29) are displayed as green crosses in Fig. 1, over the plane formed by the absolute value of the vector $\boldsymbol{\epsilon}$ and the squared root of the absolute value of the alignment vector $\boldsymbol{\Lambda}$, with both quantities measured in GeV. Two distinctive regions are observed, with low and high values of $|\boldsymbol{\Lambda}|$, with solution

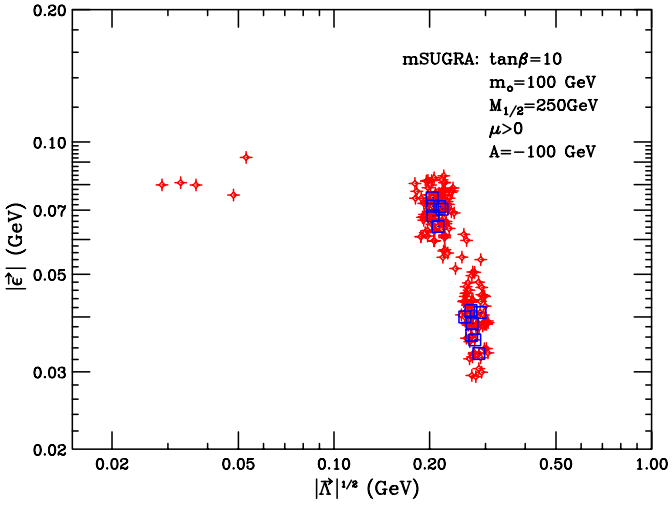

Fig. 1. Solutions to neutrino physics passing all experimental cuts described in the text, working within a particular supergravity benchmark

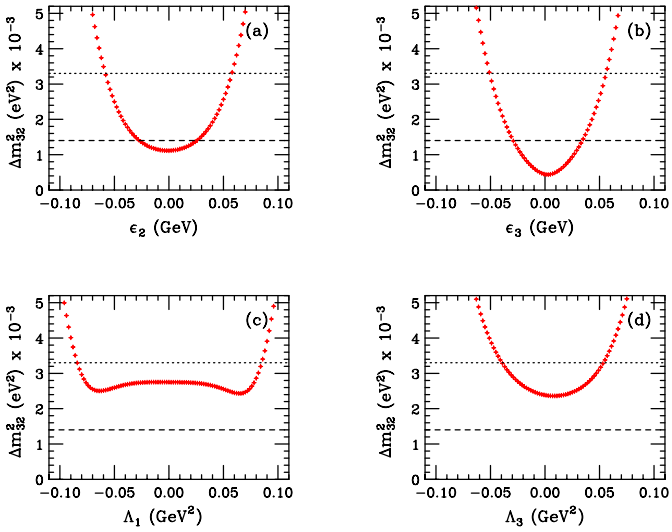

Fig. 2a–d. Atmospheric mass-squared difference as a function of the four relevant BRpV parameters for the reference scenario: ϵ_2, ϵ_3, Λ_1, and Λ_3

with a low value of $|\boldsymbol{\Lambda}|$ being harder to obtain. When the stringent cuts are implemented we find solutions only in the region of large $|\boldsymbol{\Lambda}|$, and we represent them as blue squares.

Since the tree-level neutrino mass matrix depends on Λ_i only, and one-loop corrections depend on both Λ_i and ϵ_i, although dominated by ϵ_i, the position of the solutions in the plane $|\boldsymbol{\epsilon}|$ versus $|\boldsymbol{\Lambda}|$ is an indication of how important loop contributions are. We stress the fact, nevertheless, that increasing values of $\tan\beta$ (which we keep constant in this study) increase the importance of one-loop corrections, as observed in (21) due to the presence of the Yukawa couplings. In our case, as we will confirm in the following figures, the one-loop contributions to the neutrino mass matrix are very important.

In Fig. 2 we have the atmospheric mass-squared difference as a function of the four BRpV parameters ϵ_2, ϵ_3, Λ_1, and Λ_3. The neutrino mass matrix has the texture shown in (15), which implies an atmospheric squared mass difference Δm^2_{32} given approximately by (20). The parameters m and a in (15) are $m = A\Lambda_3^2 + C\epsilon_3^2$ and $a = C\epsilon_2^2/m$, as can be read from (28). The scale m is quadratic in the parameters Λ_3 and ϵ_3, since the dependence of A and C on the Λs and ϵs is weak. The dependence of the atmospheric mass is obtained by replacing these expressions in (20), but when $a \approx 1/2$ the atmospheric scale can be approximated even further obtaining,

$$\Delta m^2_{32} \approx \tfrac{3}{2}\sqrt{5}(A\Lambda_3^2 + C\epsilon_3^2)C\epsilon_2^2 \tag{30}$$

explaining the quadratic dependency of Δm^2_{32} on ϵ_2, ϵ_3 and Λ_3, in frames 2a, 2b, and 2d respectively, and the mild dependency on Λ_1 (hidden in the neglected terms of order λ^2), as can be observed in frame 2c. The dependence on Λ_1 become strong at high values of this parameter because, in that case, neglected terms are no longer small.

We note that using the tree-level formulae in Sect. 2, the atmospheric mass scale would be given by $\Delta m^2_{32} \approx (A^{(0)}|\boldsymbol{\Lambda}|^2)^2 \approx 0.3 \times 10^{-3}\,\mathrm{eV}^2$, highlighting the inadequacy

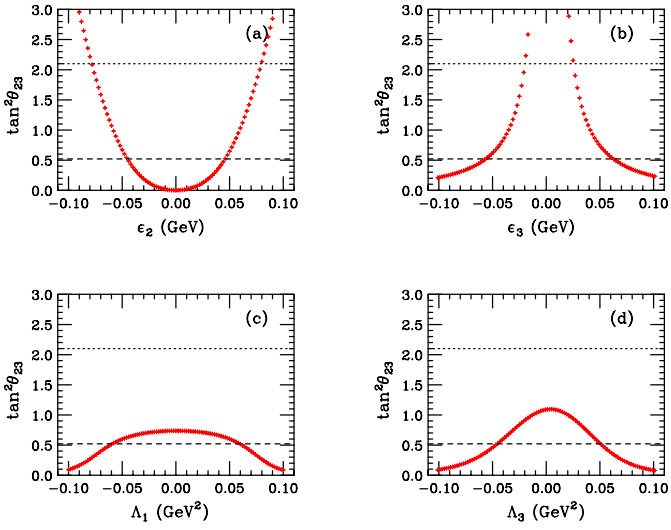

Fig. 3a–d. Atmospheric angle as a function of the four relevant BRpV parameters for the reference scenario: ϵ_2, ϵ_3, Λ_1, and Λ_3

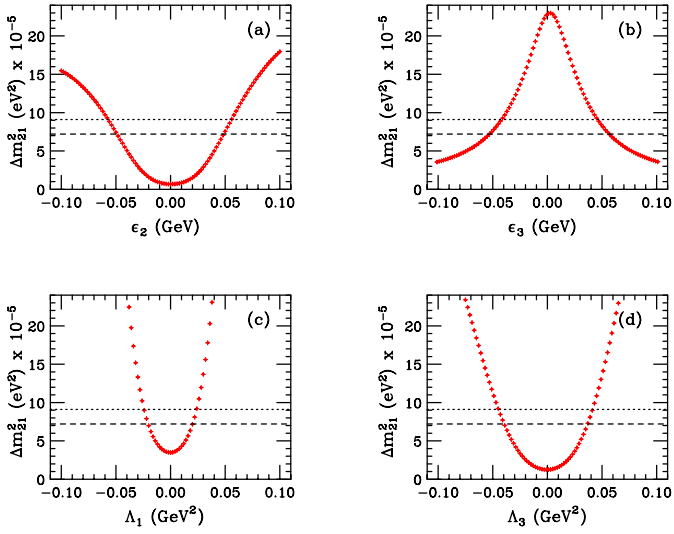

Fig. 4a–d. Solar mass squared difference as a function of the four relevant BRpV parameters for the reference scenario: ϵ_2, ϵ_3, Λ_1, and Λ_3

of the tree-level formula. On the contrary, the approximated expression in (30) gives a value of $2.8 \times 10^{-3}\,\mathrm{eV}^2$, which is much closer to the value in (14) found using the complete calculation.

In Fig. 3 we plot the tangent squared of the atmospheric angle, $\tan^2\theta_{23}$. Using (19), or directly from the mass matrix in (28), we find that the atmospheric angle satisfies

$$\tan 2\theta_{23} \approx \frac{2C\epsilon_2\epsilon_3}{A\Lambda_3^2 + C(\epsilon_3^2 - \epsilon_2^2)}\,. \tag{31}$$

This relation implies that, if ϵ_2 approaches zero, the atmospheric angle $\theta_{23} \to 0$. This behavior is confirmed in frame 3a. On the other hand, if ϵ_3 approaches zero then $\theta_{23} \to \pi/2$ because $C\epsilon_2^2$ is larger than $A\Lambda_3^2$, and this explains the divergence of $\tan\theta_{23}$ in frame 3b.

In frame 3c we see again the mild dependency of the atmospheric parameters on Λ_2, in this case the atmospheric angle. If this parameter becomes very large though, neglected terms of order λ^2 become important. Finally, the dependency of the atmospheric angle on Λ_3 in frame 3d can also be understood from (31) since clearly if $|\Lambda_3|$ grows then $\tan\theta_{23}$ decreases.

From (9), the tree-level atmospheric angle satisfies

$$\tan 2\theta_{23}^{(0)} = \frac{2\Lambda_2\Lambda_3}{\Lambda_3^2 - \Lambda_2^2} \tag{32}$$

and this relation clearly misses all the influence of the one-loop graphs on the neutrino mass matrix seen in (31). Numerically, the approximated formula in (31) gives $\tan^2\theta_{23} \approx 0.42$, which is close to the value in (14). On the contrary, the tree-level formula implies $\tan^2\theta_{23}^{(0)} \approx 0$.

In Fig. 4 we plot the solar mass squared difference as a function of the BRpV parameters ϵ_2, ϵ_3, Λ_1, and Λ_3. In the case of Δm^2_{21} the neglected terms of order λ^2 in (20) are numerically more important than in the atmospheric case; therefore, predictions based on this approximation are less accurate.

In frame 4a we see the dependence of the solar mass on ϵ_2. This behavior can be understood considering that the parameter a is proportional to ϵ_2^2, and when this parameter goes to zero, the solar mass difference approaches zero like a^2, as seen from (20).

In frame 4b we see how the solar mass difference depends on ϵ_3. If $\epsilon_3 \to 0$ then the eigenvalue $C\epsilon_2^2$ decouples and becomes the heaviest neutrino. Of the other two, one neutrino is massless, and the solar mass difference becomes equal to the second neutrino mass squared. A growing ϵ_3 will mix the massless neutrino with the heaviest, increasing the lightest neutrino mass, therefore, decreasing the solar mass difference, as observed in frame 4b.

The dependency of the solar mass on Λ_1 and Λ_3 can be understood only if we go beyond the simple approximation in (20). Terms of order λ^2 introduce a dependency on Λ_1 and Λ_3 such that λ approaches zero when these last parameters go to zero, thus explaining the behavior shown in frame 4c and 4d.

In Fig. 5 we have the tangent squared of the solar angle, $\tan^2\theta_{12}$, as a function of the BRpV parameters ϵ_2, ϵ_3, Λ_1, and Λ_3. Working in the texture given in (15), the solar angle according to (19) is approximately given by

$$\tan\theta_{12} = \frac{A\Lambda_1^2}{m_{\nu_2}} \sin\theta_{23}\,. \tag{33}$$

The dependency on Λ_1 is explicit and comes from the small parameter λ in (15). As we know from (19) and (20), the dependency of θ_{23} and m_{ν_2} on Λ_1 is weak. The behavior of the solar angle on Λ_1 seen in frame 5c is thus understood.

The solar angle as a function of ϵ_2 can also be easily understood noting that the parameter a is directly proportional to ϵ_2^2. According to (16) and (19) the second neutrino mass approaches zero when $a \to 0$, explaining the divergence shown in frame 5a. Note that $\sin\theta_{23}$ also approaches zero when $\epsilon_2 \to 0$, but more slowly.

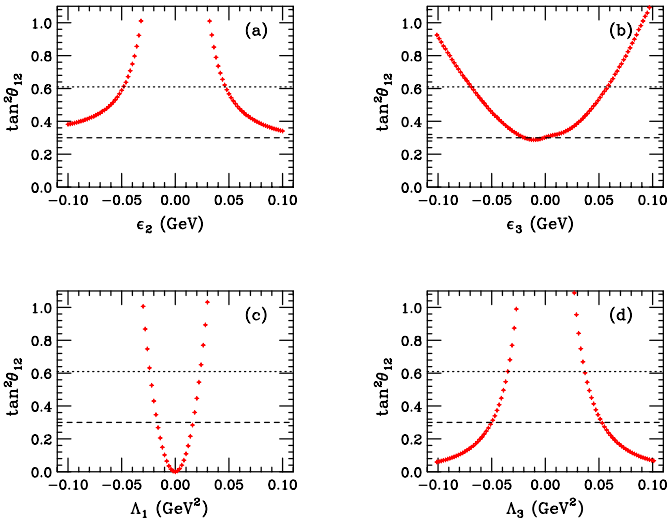

Fig. 5a–d. Tangent squared of the solar angle as a function of the four relevant BRpV parameters for the reference scenario: ϵ_2, ϵ_3, Λ_1, and Λ_3

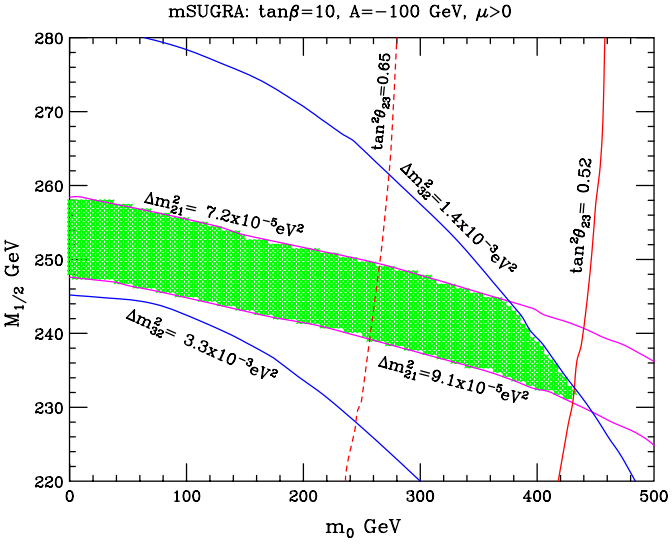

Fig. 6. Region of parameter space in the plane $m_0 - M_{1/2}$ where solutions to neutrino physics passing all the implemented experimental cuts are located. Contours of constant atmospheric mass difference and angle, and solar mass difference are displayed

The divergence of $\tan\theta_{12}$ when $\Lambda_3 \to 0$ is harder to understand from the approximated expression in (33), so we go back to the effective neutrino mass matrix in (28). If Λ_3 approaches zero then the upper-left element of the matrix decouples with a mass $A\Lambda_1^2$. On the other hand, the lower-right 2×2 sub-matrix has a zero eigenvalue, implying that $\theta_{12} \to \pi/2$, and therefore explaining the divergence shown in frame 5d.

In Fig. 6 we have chosen the neutrino solution given by the BRpV parameters in (13), and vary the scalar mass m_0 and the gaugino mass $M_{1/2}$, looking for solutions that satisfy all experimental cuts. In this case, Sugra points satisfying the experimental restrictions on the neutrino parameters lie in the shaded region. Solutions are concentrated in a narrow band defined by $M_{1/2} \approx 230$–$260\,\mathrm{GeV}$ and $m_0 \approx 0$–$400\,\mathrm{GeV}$. We note that in BRpV the LSP need not to be the lightest neutralino, since it is not stable anyway. For this reason, the region close to $m_0 \approx 0$ is not ruled out.

Smaller values of $M_{1/2}$ are not possible because the atmospheric and solar mass differences become too large. The allowed strip is, thus, limited from below by the curve $\Delta m^2_{21} = 9.1\times10^{-5}\,\mathrm{eV}^2$. The dependency on $M_{1/2}$ is felt stronger by the tree-level contribution to the parameter A, given in (26). There we see that A decreases when the gaugino mass $M_{1/2}$ increases, implying that the atmospheric mass decreases with $M_{1/2}$, as seen in (30). In addition, the solar mass difference is proportional to the parameter m^2, which in turn is proportional to A, thus, the solar mass also decreases with the gaugino mass.

Higher values of the scalar mass m_0 are not allowed because the atmospheric angle becomes too small. The allowed strip is, therefore, limited on the right by the contour $\tan^2\theta_{23} = 0.52$. We can understand this behavior in the following way: the parameter C decreases with increasing m_0 due to the Veltman's functions, and this in turn makes $\tan^2\theta_{23}$ decrease with the scalar mass. High values of the scalar mass are also limited from above because the atmospheric mass becomes too large. This can be explained from (30) considering that the parameter C decreases with increasing m_0.

Higher values of $M_{1/2}$ are not possible because the solar mass becomes too small, therefore, the allowed stripe is limited from above by the line $\Delta m^2_{21} = 7.2\times10^{-5}\,\mathrm{eV}^2$. As we already mentioned, the solar mass difference is proportional to the parameter m^2, which in turn is proportional to A, and we already know that A decreases with increasing gaugino mass $M_{1/2}$.

In Fig. 7 we see from another point of view the dependence of the solar and atmospheric mass differences on the

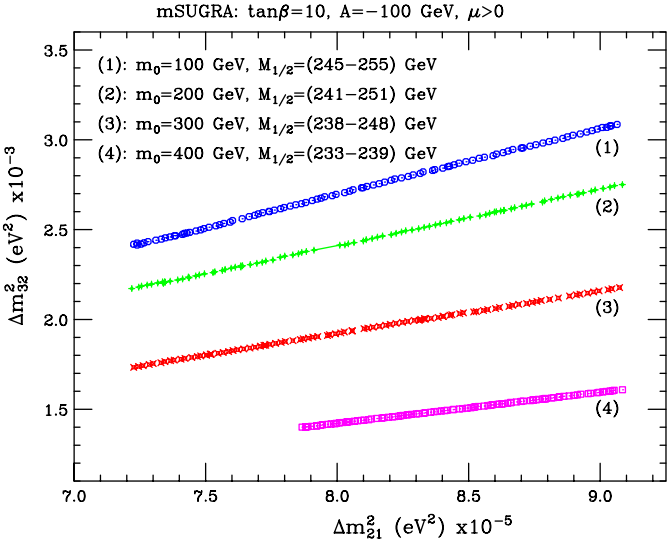

Fig. 7. Solutions to neutrino physics in the plane formed with the atmospheric and the solar mass differences. For the three different values of m_0 =100, 150, and 200 GeV, we vary the gaugino mass $M_{1/2}$

scalar mass m_0, and the gaugino mass $M_{1/2}$. In the plane formed by the atmospheric and solar mass differences we plot four curves defined by a constant value of the scalar mass $m_0 = 100, 200, 300$, and $400\,\mathrm{GeV}$, and vary the gaugino mass in its allowed region, which is indicated in the figure. We keep fixed the values of the BRpV parameters ϵ_i and Λ_i, given (13). The two neutrino mass differences are clearly proportional to each other, highlighting their common origin represented by (25), where the parameter A is controlled by tree-level physics and the parameter C is controlled by one-loop physics, and where both are equally important. Figure 7 can be understood further when seen in relation with Fig. 6.

7 Collider physics

In our model, lepton number and R-parity are not conserved. One important consequence is that the lightest supersymmetric particle (LSP) is not stable, and will decay into SM particles. Since it is not stable, the LSP need not be the lightest neutralino, and whatever it is, its decays can be used to prove the BRpV parameters and the neutrino properties [10]. In the supergravity benchmark point considered here, the LSP is the lightest neutralino, with a mass of $m_{\chi_1^0} = 99\,\mathrm{GeV}$.

One of the interesting decay modes of the neutralino is $\chi_1^0 \to W^{\pm} l^{\mp}$, where $l = e, \mu, \tau$. This decay is possible because the neutralino mixes with neutrinos, which in turn couple to the pair Wl, and also because the charged leptons mix with charginos and they in turn couple to the pair $\chi_1^0 W$. For this reason, the relevant couplings in this decay are in general very dependent on ϵ_i and Λ_i. In Fig. 8 we plot

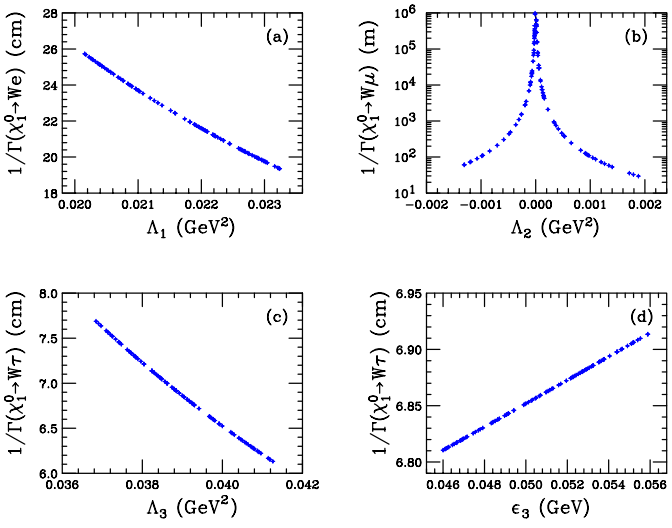

Fig. 8a–d. Partial decay width of a neutralino into a W and a lepton, measured in units of distance

the inverse of the partial decay width (multiplied by the velocity of light to convert it into a distance) as a function of the most relevant BRpV parameters. In frame 8a we see the inverse of $\Gamma(\chi_1^0 \to We)$ as a function of Λ_1. In fact, for all practical purposes, the decay rate into electrons depends *only* on Λ_1. Since in the first approximation, the coupling is proportional to Λ_1, the inverse of the decay rate behaves like Λ_1^{-2}, and this is seen in the figure. The values of Λ_1 are limited by the solar parameters. The inverse of the partial decay rate $\chi_1^0 \to We$ is of the order of 20–25 cm, and it is an important part of the total decay rate.

In frame 8b we have the inverse of $\Gamma(\chi_1^0 \to W\mu)$ as a function of Λ_2, and similarly to the previous case, the decay rate into muons depends practically only on Λ_2. In our reference model in (13) we have $\Lambda_2 \approx 0$, but values indicated in the figure are also compatible with neutrino physics. The coupling of the neutralino to W and muon is proportional to Λ_2, so the inverse of the decay rate goes like Λ_2^{-2}, as observed in frame 8b. Depending on the value of Λ_2, the partial decay length vary from centimeters to kilometers in the figure. Therefore, this partial decay rate contributes little to the total decay rate of the neutralino.

The inverse of $\Gamma(\chi_1^0 \to W\tau)$ is plotted in frames 8c and 8d as a function of Λ_3 and ϵ_3 respectively. The dependence on Λ_3 is stronger and, similarly to the previous cases, it goes like Λ_3^{-2}. The dependence on ϵ_3 is weaker, and the inverse decay rate increases with this parameter. The inverse decay rate is of the order of 7 cm, making it the most important contribution to the total decay rate. Including the decay modes into neutrinos and a Z, the total inverse decay rate is near 4 cm. The ratios of branching ratios for our benchmark point in (13) are given by

$$\frac{B(\chi_1^0 \to W\mu)}{B(\chi_1^0 \to W\tau)} = 5.9 \times 10^{-5}\,, \quad \frac{B(\chi_1^0 \to We)}{B(\chi_1^0 \to W\tau)} = 0.32\,. \tag{34}$$

We note that if we increase Λ_2 by a factor of four, the first ratio of branching ratios increase to $\sim 10^{-3}$ without changing the other ratio, while still passing all the experimental cuts. In this way, it is clear that by measuring the branching ratios of the neutralinos we get information on the parameters of the model.

The discussion above suggests that the observation of events coming from processes like $pp \to \chi_1^0\chi_1^0 \to WWe\tau$ (at the LHC) or $e^+e^- \to \chi_1^0\chi_1^0 \to WWe\tau$ (at the NLC) would make it possible to measure parameters relevant for neutrino physics.

We used CompHEP 4.4 [24] to calculate the production cross sections $\sigma(pp \to \chi_1^0\chi_1^0)$ (LHC) and $\sigma(e^+e^- \to \chi_1^0\chi_1^0)$ (NLC at $\sqrt{s} = 500\,\mathrm{GeV}$) at leading order. The relevant Feynman diagrams for the LHC are shown in Fig. 9. For the SPS1 mSugra benchmark we obtain:

$$\begin{aligned} \sigma\left(pp \to \chi_1^0\chi_1^0\right) &= 9.8 \times 10^{-3}\,\mathrm{pb}\,, \\ \sigma\left(e^+e^- \to \chi_1^0\chi_1^0\right) &= 0.27\,\mathrm{pb}\,. \end{aligned} \tag{35}$$

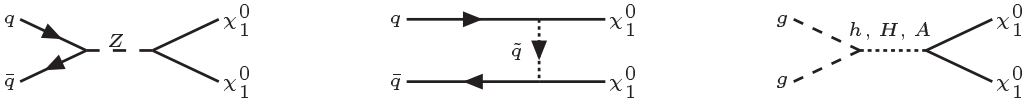

Fig. 9. Feynman diagrams relevant for the production of two neutralinos at the LHC

The cross sections of the whole processes were calculated by multiplying the production cross sections by the branching ratios $B(\chi_1^0 \to W^+ e^-)$ and $B(\chi_1^0 \to W^+ \tau^-)$. Their values, for the set of parameters we have chosen, are:

$$\begin{aligned} B\left(\chi_1^0 \to W^+ e^-\right) &= 0.10 \\ B\left(\chi_1^0 \to W^+ \tau^-\right) &= 0.33\,. \end{aligned} \tag{36}$$

The complete cross sections are:

$$\begin{aligned} \sigma\big(pp \to \chi_1^0\chi_1^0 \to W^+W^+e^-\tau^-\big) &= 3.4 \times 10^{-4}\,\mathrm{pb}\,, \\ \sigma\big(e^+e^- \to \chi_1^0\chi_1^0 \to W^+W^+e^-\tau^-\big) &= 9.3 \times 10^{-3}\,\mathrm{pb}\,. \end{aligned} \tag{37}$$

On the other hand, the main source of background comes from the production of four Ws with two of them decaying leptonically. We calculated those processes using CompHEP and we found:

$$\begin{aligned} &\sigma\left(pp \to WWWW \to W^+W^+e^-\tau^-\bar{\nu_e}\bar{\nu_\tau}\right) \\ &= 6.5 \times 10^{-6}\,\mathrm{pb}\,, \\ &\sigma\left(e^+e^- \to WWWW \to W^+W^+e^-\tau^-\bar{\nu_e}\bar{\nu_\tau}\right) \\ &= 1.6 \times 10^{-6}\,\mathrm{pb}\,. \end{aligned} \tag{38}$$

Assuming a luminosity of $10^5\,\mathrm{pb}^{-1}$/year at both the LHC and the NLC, we expect ~ 70 signal event per year at the LHC and ~ 930 signal events per year. Nevertheless we are not interested in the charge of the final leptons, we only require that one lepton belongs to the first family and the other to the third one, so the total number of signal events is obtained by multiplying the above results by four.

We remark that, while the background is small in both cases, the number of signal events at the LHC is also small, specially if a less-optimistic luminosity is used, in which case a more detailed analysis is required. On the other hand the NLC appears to be a very auspicious environment for studying this model.

8 Conclusions

We have reexamined the possibility of generating neutrino masses and mixing angles in supergravity with non-universal bilinear R-parity-violating parameters. We found solutions with a relatively large value of $\tan\beta$, such that one-loop contributions to the neutralino mass matrix are as important as tree-level contributions. The heaviest neutrino mass is still generated mainly at the tree level, but the other two masses and the three mixing angles are strongly affected by loops. In particular, the tree-level approximations for the mixing angles give completely erroneous results.

We concentrate our study on a texture for the neutrino mass matrix which is common among our solutions, and on one particular solution corresponding to this texture. The atmospheric mixing is nearly maximal, and the deviation of the parameter $\tan^2\theta_{23}$ from unity is related to the small size of the ratio between the solar and atmospheric mass scales $\Delta m^2_{sol}/\Delta m^2_{atm}$. In addition, the solar and reactor angles are both small because of the small parameter λ, which in turn is small because $\Lambda_1/\Lambda_3 < 1$. Nevertheless, the reactor angle is much smaller than the solar angle because the second neutrino mass is much larger than the third one.

We have shown how the neutrino observables depend on the BRpV parameters ϵ_i and Λ_i, and this dependency can be understood in terms of simple approximations in terms of parameters A, B, and C, where all the complication of the one-loop contributions is concentrated. The dependency on ϵ_i and Λ_i is strong, and it is not clear a priori that a solution is available, due to the increasing precision of the measurements of the neutrino observables. It is also shown how these observables depend on the Sugra parameters, namely the universal scalar mass m_0 and the universal gaugino mass $M_{1/2}$. For the given values of ϵ_i and Λ_i, solutions lie in a narrow strip in the plane $m_0 - M_{1/2}$, where the gaugino mass is strongly restricted by the solar and atmospheric mass scales, and the scalar mass by the atmospheric angle and mass scale.

Finally, we showed how the decay rates of the neutralino depend directly on some of the parameters ϵ_i and Λ_i. In fact $\Gamma(\chi_1^0 \to We)$ and $\Gamma(\chi_1^0 \to W\mu)$ depend *only* on Λ_1 and Λ_2 respectively, while $\Gamma(\chi_1^0 \to W\tau)$ depends on both Λ_3 and ϵ_3. Measurements on branching ratios of the LSP can therefore give important information on the parameters of the model. We estimated that a ~ 70 events with $e^-\tau^-$ in the final state can be observed at the LHC and ~ 930 at the LC, indicating that a measurement of the decay rates is possible at the LC. A more detailed analysis is necessary to estimate the expected precision of these measurements.

Acknowledgements. This research was partly founded by CONICYT grants Nos. 1030948 and 1040384.

References

1. Y. Fukuda et al. [Super-Kamiokande Collaboration], Phys. Rev. Lett. **81**, 1562 (1998); Q.R. Ahmad et al. [SNO Collaboration], Phys. Rev. Lett. **89**, 011301 (2002); K. Eguchi et al. [KamLAND Collaboration], Phys. Rev. Lett. **90**, 021802 (2003); Y. Fukuda et al. [Super-Kamiokande Collaboration], Phys. Rev. Lett. **82**, 1810 (1999)
2. W. Grimus, arXiv:hep-ph/0307149; G. Altarelli and F. Feruglio, arXiv:hep-ph/0306265
3. T. Yanagida, in: Proceedings of the Workshop on Unified Theory and Baryon Number in the Universe, KEK, 1979; M. Gell-Mann, P. Ramond, R. Slansky, in: Supergravity (Stony Brook, 1979); R.N. Mohapatra, G. Senjanovic, Phys. Rev. Lett. **44**, 912 (1980)
4. M. Hirsch, J.W.F. Valle, arXiv:hep-ph/0405015
5. G.R. Farrar and P. Fayet, Phys. Lett. B **76**, 575 (1978)
6. M. Chemtob, arXiv:hep-ph/0406029; R. Barbier et al., arXiv:hep-ph/0406039; B. Allanach et al. [R parity Working Group Collaboration], arXiv:hep-ph/9906224; B.C. Allanach et al., J. Phys. G **24**, 421 (1998)
7. A.G. Akeroyd, et al., Nucl. Phys. B **529**, 3 (1998); A. Abada, S. Davidson, M. Losada, Phys. Rev. D **65**, 075010 (2002); M.A. Diaz, J. Ferrandis, J.C. Romao,

J.W.F. Valle, Phys. Lett. B **453**, 263 (1999); S.Y. Choi, E.J. Chun, S.K. Kang, J.S. Lee, Phys. Rev. D **60**, 075002 (1999); A.G. Akeroyd, M.A. Diaz, J.W.F. Valle, Phys. Lett. B **441**, 224 (1998); O. Haug, J.D. Vergados, A. Faessler, S. Kovalenko, Nucl. Phys. B **565**, 38 (2000); M.A. Diaz, E. Torrente-Lujan, J.W.F. Valle, Nucl. Phys. B **551**, 78 (1999); A.S. Joshipura, R.D. Vaidya, S.K. Vempati, Nucl. Phys. B **639**, 290 (2002); S.K. Kang, O.C.W. Kong, Phys. Rev. D **69**, 013004 (2004)

8. D.F. Carvalho, M.E. Gomez, J.C. Romao, Phys. Rev. D **65**, 093013 (2002); M.A. Diaz, J. Ferrandis, J.C. Romao, J.W.F. Valle, Nucl. Phys. B **590**, 3 (2000); Y. Grossman, H.E. Haber, Phys. Rev. D **63**, 075011 (2001); M.A. Diaz, J. Ferrandis, J.W.F. Valle, Nucl. Phys. B **573**, 75 (2000); F. De Campos et al., Nucl. Phys. B **623**, 47 (2002); M.A. Diaz, R.A. Lineros, M.A. Rivera, Phys. Rev. D **67**, 115004 (2003); R. Kitano, K.Y. Oda, Phys. Rev. D **61**, 113001 (2000); A.G. Akeroyd, E.J. Chun, M.A. Diaz, D.W. Jung, Phys. Lett. B **582**, 64 (2004); F. Takayama, M. Yamaguchi, Phys. Lett. B **476**, 116 (2000); F. de Campos et al., arXiv:hep-ph/0409043
9. M.A. Diaz, in: Proceedings of Valencia 1997, Beyond the Standard Model: From Theory to Experiment, pp. 188–199, arXiv:hep-ph/9802407
10. J.C. Romao, M.A. Diaz, M. Hirsch, W. Porod, J.W.F. Valle, Phys. Rev. D **61**, 071703 (2000)
11. M. Hirsch, M.A. Diaz, W. Porod, J.C. Romao, J.W.F. Valle, Phys. Rev. D **62**, 113008 (2000); Erratum Phys. Rev. D **65**, 119901 (2002)
12. P. Nogueira, J.C. Romao, J.W.F. Valle, Phys. Lett. B **251**, 142 (1990); M.C. Gonzalez-Garcia, J.W.F. Valle, Nucl. Phys. B **355**, 330 (1991); J.C. Romao, J.W.F. Valle, Nucl. Phys. B **381**, 87 (1992); M.C. Gonzalez-Garcia, J.C. Romao, J.W.F. Valle, Nucl. Phys. B **391**, 100 (1993); J.C. Romao, F. de Campos, J.W.F. Valle, Phys. Lett. B **292**, 329 (1992); J.C. Romao, F. de Campos, M.A. Garcia-Jareno, M.B. Magro, J.W.F. Valle, Nucl. Phys. B **482**, 3 (1996)
13. J.M. Mira, E. Nardi, D.A. Restrepo, J.W.F. Valle, Phys. Lett. B **492**, 81 (2000) [arXiv:hep-ph/0007266]
14. A. Kogut et al., Astrophys. J. Suppl. **148**, 161 (2003)
15. H.V. Klapdor-Kleingrothaus, A. Dietz, H.L. Harney, I.V. Krivosheina, Mod. Phys. Lett. A **16**, 2409 (2001); C.E. Aalseth et al., Mod. Phys. Lett. A **17**, 1475 (2002)
16. H. Nunokawa, W.J.C. Teves, R. Zukanovich Funchal, Phys. Lett. B **562**, 28 (2003); P.C. de Holanda, A.Y. Smirnov, JCAP **0302**, 001 (2003); P. Aliani, V. Antonelli, M. Picariello, E. Torrente-Lujan, Phys. Rev. D **69**, 013005 (2004); J.N. Bahcall, M.C. Gonzalez-Garcia, C. Pena-Garay, JHEP **0302**. 009 (2003); G.L. Fogli, E. Lisi, A. Marrone, D. Montanino, A. Palazzo, A.M. Rotunno, Phys. Rev. D **67**, 073002 (2003); V. Barger, D. Marfatia, Phys. Lett. B **555**, 144 (2003); A. Bandyopadhyay, S. Choubey, R. Gandhi, S. Goswami, D.P. Roy, Phys. Lett. B **559**, 121 (2003)
17. M. Maltoni, T. Schwetz, M.A. Tortola, J.W.F. Valle, arXiv:hep-ph/0405172
18. A. Djouadi, J.L. Kneur, G. Moultaka, arXiv:hep-ph/0211331
19. N. Ghodbane, H.U. Martyn, arXiv:hep-ph/0201233
20. H.V. Klapdor-Kleingrothaus, arXiv:hep-ph/0307330
21. M.A. Diaz, M. Hirsch, W. Porod, J.C. Romao, J.W.F. Valle, Phys. Rev. D **68**, 013009 (2003) [arXiv:hep-ph/0302021]
22. A.Y. Smirnov, arXiv:hep-ph/0402264; R.N. Mohapatra, arXiv:hep-ph/0402035
23. M. Hirsch, W. Porod, Phys. Rev. D **68**, 115007 (2003); A. Bartl, M. Hirsch, T. Kernreiter, W. Porod, J.W.F. Valle, JHEP **0311**, 005 (2003); M.B. Magro, F. de Campos, O.J.P. Eboli, W. Porod, D. Restrepo, J.W.F. Valle, JHEP **0309**, 071 (2003); D. Restrepo, W. Porod, J.W.F. Valle, Phys. Rev. D **64**, 055011 (2001); D.W. Jung, S.K. Kang, J.D. Park, E.J. Chun, arXiv:hep-ph/0407106; Phys. Rev. D **66**, 073003 (2002); M.A. Diaz, D.A. Restrepo, J.W.F. Valle, Nucl. Phys. B **583**, 182 (2000); A. Belyaev, M.H. Genest, C. Leroy, R.R. Mehdiyev, arXiv:hep-ph/0401065; D. Aristizabal Sierra, M. Hirsch, W. Porod, arXiv:hep-ph/0409241; E.J. Chun, J.S. Lee, Phys. Rev. D **60**, 075006 (1999)
24. CompHEP – a Package for the Evaluation of Feynman Diagrams and Integration over Multi-Particle Phase Space, User's Manual for Version 3.3, hep-ph/9908288; E. Boos, V. Bunichev, M. Dubinin, L. Dudko, V. Ilyin, A. Kryukov, V. Edneral, V. Savrin, A. Semenov, A. Sherstnev, COMPHEP 4.4 – Automatic Computations From Lagrangians To Events (2004), hep-ph/0403113; Home page: http://theory.sinp.msu.ru/comphep